ESA CONTRACT REPORT

Contract Report to the European Space Agency

FASTEM - SMOS Evaluation

Authors: Giovanna De Chiara, Lars Isaksen, Stephen English

Report for ESA contract 4000101703/10/NL/FF/fk CCN6

Work Package 400 - Technical Report 1 (TR1)

European Centre for Medium-Range Weather Forecasts
Europäisches Zentrum für mittelfristige Wettervorhersage
Centre européen pour les prévisions météorologiques à moyen terme

ECMWF

Series: ECMWF - ESA Contract Report

A full list of ECMWF Publications can be found on our web site under:

http://www.ecmwf.int/publications/

European Centre for Medium Range Weather Forecasts Shinfield Park, Reading, RG2 9AX, England

Contract Report to the European Space Agency

FASTEM - SMOS Evaluation

Authors: Giovanna De Chiara, Lars Isaksen and Stephen English

Technical Report for ESA contract 4000101703/10/NL/FF/fk
CCN6 – WP400

European Centre for Medium-Range Weather Forecasts
Shinfield Park, Reading, Berkshire, UK

August 2019

TABLE OF CONTENTS

Abbreviations ..... **ii**

1. Introduction **1**

2. RTTOV- FASTEM **2**

3. CMEM **3**

4. SMOS observations **3**

4.1. SMOS observed brightness temperature 5

5. SMOS simulated Tb with RTTOV-FASTEM **9**

5.1. FASTEM versus CMEM 9

5.2. Setting up FASTEM 9

5.3. FASTEM simulated brightness temperature 12

6. SMOS-FASTEM departures **14**

7. FASTEM vs CMEM variability **21**

8. Conclusions **23**

Acknowledgements **24**

References

Abbreviations

BG ..... Background
CMEM ……. Community Microwave Emission Modelling Platform
DPGS ..... Data Processing Ground Segment
ECMWF ..... European Centre for Medium-range Weather Forecasts
ESA ..... European Space Agency
ESAC ..... European Space Astronomy Centre
FASTEM ..... FAST microwave Emissivity Model
IFREMER ..... Institut français de recherche pour l'exploitation de la mer
IFS ..... Integrated Forecasting System
GMF ..... Geophysical Model Function
NetCDF ..... Network Common Data Format
NRT ..... Near Real Time
ODB ..... ECMWF Observational DataBase
OTT ..... Ocean Target Transformation
QC ..... Quality Control
RFI ..... Radio Frequency Interferences
RTTOV ..... Radiative Transfer for TOVS
SMOS ..... Soil Moisture and Ocean Salinity
SSS ..... Sea Surface Salinity
TB ..... Brightness Temperatures
TC ..... Tropical Cyclone

Abstract

L-band SMOS brightness temperature measurements have been monitored for a long time at ECMWF using the Community Microwave Emission Modelling Platform (CMEM) forward model. CMEM is a well-established model to simulate L-band measurement over land. Over inland water bodies, coastal areas and open ocean, instead, a simplified emissivity model is used that does not account for the wind and foam dependent emissivity changes. L-band measurements over the ocean are known to be sensitive to high winds and could provide Numerical Weather Prediction (NWP) systems with wind information not given by other higher frequency passive measurements or active instruments.

In this study a preliminary analysis is carried out to investigate the use of an alternative forward model operator, RTTOV-FASTEM, over the ocean. RTTOV is widely used in the NWP community to simulate brightness temperature for high frequency passive instruments. FASTEM is the ocean emissivity model that recently was extended to L-band. It takes account the effects of the wind induced ocean roughness and foam on the brightness temperatures. In this study the simulated SMOS brightness temperatures over the ocean have been generated using RTTOV-FASTEM and for the first time compared to CMEM simulations. The SMOS departures have been evaluated for the two forward models.

This report presents the results of the work done in the framework of the ESA contract 4000101703/10/NL/FF/fk CCN6, WP400.

1. Introduction

The Soil Moisture and Ocean Salinity (SMOS) mission was launched by the European Space Agency (ESA) in 2009 as one of the Earth Explorer missions. The SMOS mission is based on a dual polarized radiometer that provides multi-angular L-band (1.4 GHz) brightness temperature (Tb) images of the Earth [Mecklenburg et al., 2009; Kerr et al., 2010] with a spatial resolution that ranges from 35 km to 50 km. The SMOS mission was designed to provide key observations: soil moisture for land and ocean salinity for the ocean. Over the last few years, the importance of additional SMOS observations for other applications, such as marine wind speed, was demonstrated [Reul et al., 2012] [Reul et al., 2015] based on the capability to exploit the large difference between the emissivity of foam by breaking waves and the emissivity of the foam-free ocean. At L-band the emissivity of saline water is very low; these low frequencies measurements are less affected by the atmosphere than higher frequencies and there is no loss of sensitivity due to atmospheric absorption and scattering. L-band measurements can potentially provide all-weather (near surface) information over the ocean, even at very high wind speed. Differently from other instruments like scatterometer and higher frequency passive observations, the L-band measurement sensitivity is not saturating at moderately high wind speed, so SMOS observations could be very useful to provide information in case of extreme wind conditions such as Tropical Cyclones (TC) and intense extra-tropical storms. De Chiara et al., 2018 performed a preliminary assessment of the SMOS wind speed data. In their study they showed that overall the quality of SMOS winds is good and especially the strong winds observations could provide complementary information to NWP.

ECMWF's data assimilation strategy for microwave imagers (e.g. AMSR2, GMI, SSMIS) has always been to assimilate brightness temperatures over ocean for the atmospheric analysis. The RTTOV radiative transfer model has been used that has an ocean emissivity model component called FASTEM which was extended to include the L-band capability by Liu et al., [2011] but to the best of our knowledge not compared yet to actual L-band measurements. FASTEM has the capability to model the effects of the roughness and foam at the L-band emissivity and therefore should be able to produce realistic values of brightness temperature also in case of strong winds.

ECMWF is operationally monitoring global SMOS Near Real Time (NRT) brightness temperature products [Muñoz-Sabater et al., 2011a]. The monitoring is produced separately for land and oceans. The reason is the strong contrast between the dielectric constant of water bodies and land surfaces, which in turn produces very different emissivity and observed brightness temperatures at the top of the atmosphere. Thus, monitoring SMOS data separately over land and oceans increases the sensitivity to the statistical variables [Muñoz-Sabater et al., 2011b]. The monitoring results are available on the ECMWF website[1]. The SMOS brightness temperature monitoring is based, both for land and ocean, on CMEM. The simulated brightness temperature is directly compared to the SMOS observed brightness temperature at the time of the observation. The CMEM model was developed for land applications, hence the emissivity over relevant water bodies, e.g. lakes and coastal areas, is modelled in a simplified approach where the ocean is considered as a flat surface. This is not realistic for open ocean applications where the wind-induced roughness plays an important role.

In this study we investigate the usage of RTTOV-FASTEM to model the L-band brightness temperature over the ocean. The simulated brightness temperature at the top of the atmosphere at L-band is generated with RTTOV-FASTEM and compared to the CMEM ones. The different sensitivity of the two models to the ocean surface roughness are evaluated. The FASTEM simulated brightness temperature is then compared to the observed SMOS brightness temperatures.

In the report we first provide a brief description of the RTTOV-FASTEM model (in Section 2) and the CMEM model (in Section 3). In Section 4 the SMOS observations used in this study are presented and the brightness temperature measurements analysed. Section 5 presents the simulated SMOS brightness temperatures generated by RTTOV-FASTEM and how they compare to the CMEM brightness temperatures. The SMOS-FASTEM departures are evaluated in Section 6, and the variability of FASTEM and CMEM are compared to SMOS data variability in Section 7. Conclusions are presented in Section 8.

2. RTTOV- FASTEM

RTTOV (Radiative Transfer for TOVS) is a fast radiative transfer model for simulating the radiances at the top of the atmosphere from passive visible, infrared and microwave downward-viewing satellite radiometers [Saunders et al., 2018]. RTTOV is widely used in the satellite retrieval and data assimilation communities.

Brightness temperatures at microwave frequencies are a function of surface emissivity. Over the oceans, the emissivity is further affected by surface wind speed, wind direction, water salinity, and temperature. For a flat-water surface, the reflectance can be accurately calculated from the Fresnel formula for a given water permittivity and a local incident angle. When the ocean surface becomes rough, surface reflection of radiation will be affected by various scales of ocean waves such as gravity and capillary waves. For a wind speed larger than 4–7 ms^{-1}, whitecapping occurs, leading to surface foam, and this modifies the surface reflection. For fast computations of ocean reflectivity or emissivity, a model called FAST microwave Emissivity Model (FASTEM) was developed, and it is used in remote sensing and data assimilation communities [English and Hewison, 1998]. FASTEM can be used for all passive microwave sensors and polarized and polarimetric sensors. It includes the dependence on surface wind

1 https://www.ecmwf.int/en/forecasts/quality-our-forecasts/monitoring/smos-monitoring

speed and direction, sea water salinity, and sea surface temperature. The model takes account of the reflection of downwelling atmospheric radiation, including the Cosmic Microwave Background. FASTEM has the capability to model the effects of roughness and foam on the L-band emissivity [Liu et al., 2011], based on a parametric fit to results from a two-scale emissivity model. It uses a permittivity model for saline water.

The effect of the galactic noise is not taken into account in the implementation in RTTOV.

3. CMEM

CMEM was developed at ECMWF as the forward operator model for low frequency passive microwave brightness temperatures (from 1 GHz to 20 GHz) of the surface. It is a highly modular software package for the NWP community. CMEM's physics is based on the parameterizations used in the L-Band Microwave Emission of the Biosphere (LMEB, Wigneron et al., 2007) and Land Surface Microwave Emission Model (LSMEM, Drusch et al., 2001). In CMEM the skin temperature is used as a proxy for lake and sea effective temperature. The salinity of open water is currently set to a constant value (32.5 psu). Over lake and ocean surface, the Klein and Swift (1977) parameterization for the dielectric constant of flat water surfaces of saline water is used. This means that the ocean is considered as a smooth surface and the influence of the wind is not accounted for.

The galactic noise effect is not accounted for.

4. SMOS observations

SMOS NRT products are processed at the European Space Astronomy Centre (ESAC) in Madrid (Spain) and distributed via the SMOS Data processing Ground Segment (DPGS) interface. The full NRT product contains multi-angular brightness temperatures at the top of the atmosphere in the antenna polarization frame. The full horizontal polarized brightness temperature is denoted as XX on the antenna frame or HH on the Earth reference frame. The full vertical one as YY on the antenna frame and VV on the Earth reference frame. The conversion from one reference frame to the other is performed considering two parameters: a geometric transformation and the Faraday rotation correction. These values are provided in the NRT product.

The SMOS data has to be converted from the satellite reference (X,Y) frame into the Earth reference frame (H,V) before being able to use them for retrieval of any geophysical parameter. Any forward model generates the simulated brightness temperature on the Earth reference frame. When SMOS observed Tb are compared to the simulated ones, the two values must be on the same reference frame; typically, the simulated Tb is converted from the Earth reference frame to the antenna reference frame.

One of the major problems of SMOS observations is the (Radio Frequency Interference) RFI contamination. This is caused by L-band transmitter from the Earth surface, mainly radar or communication devices [Oliva et al., 2012]. Information on the RFI contamination are provided inside the NRT product.

At L-band radiation from celestial sources contribute to the measured signal. The cosmic background radiation is the cold remnant of radiation emitted at the origin of the universe and is almost constant in space and time (2.7 K). The other two types of sources are hydrogen line emission and the continuum radiation which is due to emissions from discrete radiosources [Le Vine and Abraham, 2011]. They are

known as the galactic noise. The galactic noise varies according to the incidence and the azimuth angle, it can be strong and spatially variable. The galactic noise has a direct component and a reflected one (glint) that, on the ocean, varies based on the sea surface roughness. In the L1 SMOS products only the direct component of the galactic noise is corrected for, because this changes the calibration of the sensor. The glint effect is usually corrected in the L2 Salinity (or wind) processing based on the wind induced sea surface roughness.

The sun is another extremely strong radiation source at L-band. It can affect the measurements in two ways: one is the reflection of sun radiations by the earth-surface (sunglitter effects) and the other is the direct leakage into the antenna. Similar effects, with a much lower intensity, are caused by the moon radiation. Only the direct sun contamination is corrected for in the L1 SMOS products. The sunglitter effect is corrected in the L2 products.

The data is distributed in Binary Universal Form for the Representation of meteorological data (BUFR) following the template described in [de Rosnay et al., 2012]. The SMOS products are fetched through the acquisition chain and archived at ECMWF. SMOS products over land and ocean are routinely monitored at ECMWF. The monitoring is running at different incidence angles and at the two polarization states. For this purpose, SMOS data is fetched from the archive and go through a pre-screening process as described in [Muñoz-Sabater et al., 2013]. SMOS data is stored in an Observational Data Base (ODB), which contains all the information about the observations [Muñoz-Sabater et al., 2011]. In the monitoring process the observations are collocated to the model grid using the nearest neighbour technique. The model equivalent and background departure are then computed. The model equivalent is the simulated brightness temperature at the observation location computed using CMEM forward model. In the monitoring tool, the simulated L-band brightness temperature is rotated from the Earth reference frame to the antenna satellite frame.

The SMOS monitoring runs in NRT at ECMWF. The ODB files are stored in the ECMWF Meteorological Archival and Retrieval System (MARS). In the ODB products, most of the original information as received in the BUFR file are stored. The CMEM equivalent model value and the background departure are also stored in the ODB files. The quality control flags ODB were used to filter out low quality data. The *Snapshot Overall Quality Fields* and the *SMOS Information Flag* and were used. They are defined in Table 1 and Table 2.

To remove observations with low quality signal due to RFI or contaminated signal, it is recommended (J. Munoz Sabatier (ECMWF) and R. Crapolicchio (ESA/ESRIN), personal communication) to select only observations with the SMOS Information Flag bits 1 and 4 set to 0, bit 5 set to 1 and the Snapshot Overall Quality Field bit 1 set to 1. The observations that passed this selection are hereafter called ‘QC’ dataset.

Table 1: Snapshot Overall Quality Field	
1	Nominal (hereafter called **NOM**)
2	Degraded by SW error: any error reported by the algorithms
3	Degraded by instrument error
4	Degraded by corrupted/missing ADF

Table 2: SMOS Information Flag	
1	Pixel is affected by RFI effects as identified in the AUX_RFILST or it has exceeded the BT thresholds (hereafter called **RFI**)
2	Pixel is located in the hexagonal alias directions centred on a Sun alias (if Sun is not removed, measurement may be degraded in these directions)
3	Pixel is close to the border delimiting the Extended Alias free zone or to the unit circle replicas borders.
4	Measurement is affected by the tails of a point source RFI as identified in the AUX RFI list (tail width is dependent on the RFI expected BT, from each snapshot measurements, corresponding to 0.16 of the radius of the RFI circle flagged). This flag is hereafter called **RFT**)
5	Pixel is inside the exclusive zone of Alias free (hereafter called **ZAF**).
6	Pixel is located in a zone where a Moon alias was reconstructed
7	Pixel is located in a zone where Sun reflection has been detected
8	Pixel is located in a zone where a Sun alias was reconstructed
9	Measurement is affected by RFI effects in the corresponding polarisation as identified in the long trend analysis of telemetry data (NIR and System Temperatures)
10	Scene has not been combined with an adjacent scene in opposite polarisation during image reconstruction
11	Direct Moon correction has been performed during image reconstruction of this pixel
12	Reflected Sun correction has been performed during image reconstruction of this pixel
13	Direct Sun correction has been performed during image reconstruction of this pixel

4.1. SMOS observed brightness temperature

Before analyzing the simulated brightness temperature generated by the forward models, we looked at the SMOS observations to examine the variability of brightness temperature as function of different observation related aspects, like RFI contamination, incidence angle, position within the swath, and polarization.

Figure 1 shows the SMOS observed brightness temperature for the YY channel and incidence angles between 38 and 42 degrees. The values of the brightness temperature are between 0 and 400 K. The distribution has two peaks, one in the range 70-150 K, the second in the range 200-250 K.

To verify if very low and high values are due to data quality problems, the products were filtered using the SMOS Information Flag and Snapshot Overall Quality fields, defined above. In Figure 2 the same data is shown after the data contaminated by RFI was removed (only data with RFI and RFT flags set to 0 is displayed). There are now less observations in the lower part of the distribution (0-70 K) and in the upper part of the distribution (270-400K). As next step, we filtered out the data that lies outside the Alias Free area, the one where the Overall quality flag (NOM) was not nominal and the sea-ice contaminated observations detected with comparison to the background fields. The remaining data is shown in Figure 3. The data is mainly in the range 70-170 K with a single distribution peak around 120 K. Most of the observations with a brightness temperature above 150 K have been removed thanks to the sea-ice contamination check. Data with such high values is generally located around Antarctica and the Arctic Ocean. The observations in the range 0-100 K have been filtered out by the Alias Free area flag. Some outliers both in the lower and upper part of the distribution still remain.

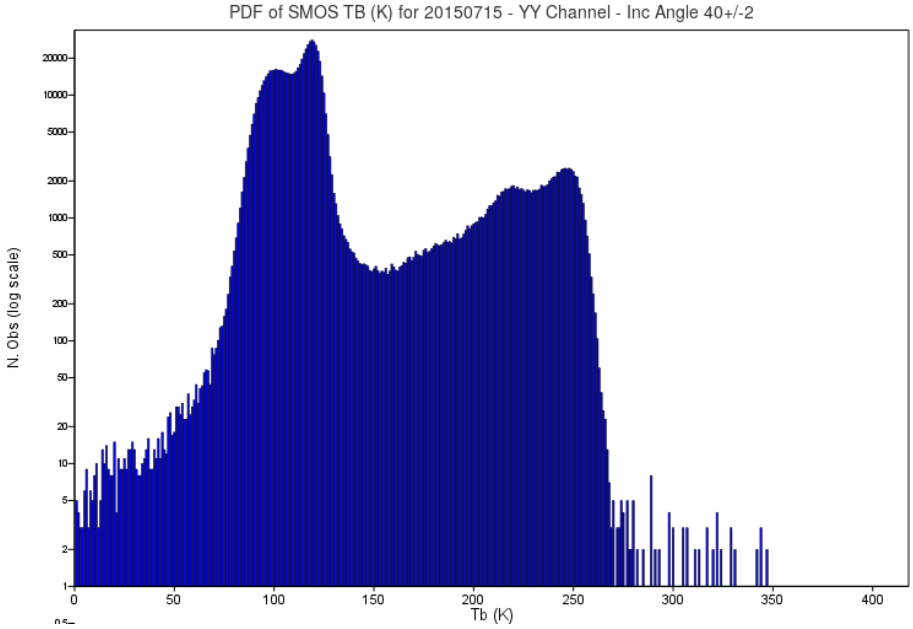

Figure 1: SMOS brightness temperature [K] data distribution on 20150715 for the YY channel and incidence angles 40°±2°.

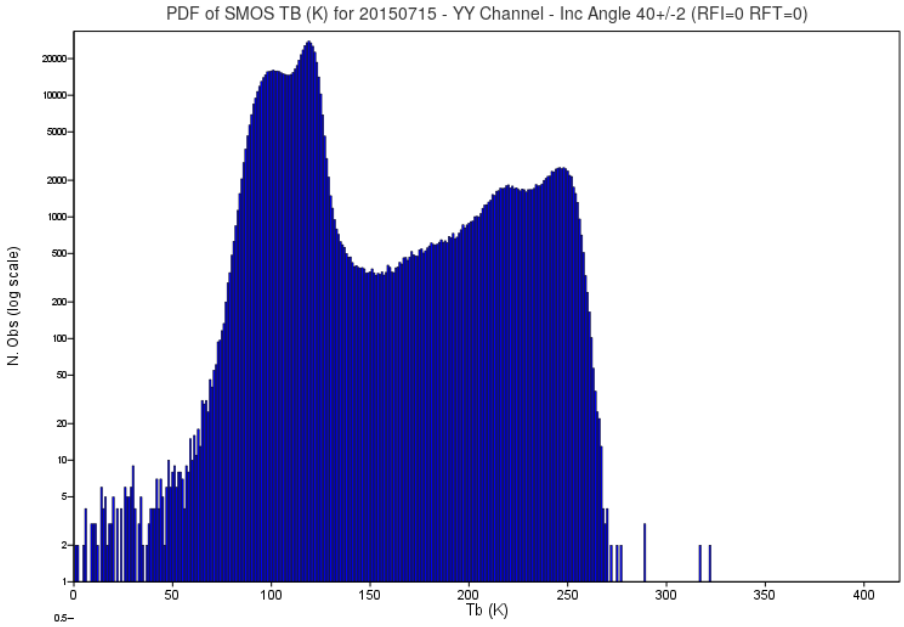

Figure 2: Similar to Fig. 1, but only where RFI and RFT flags are zero. The QC indicators are defined in Table 1.

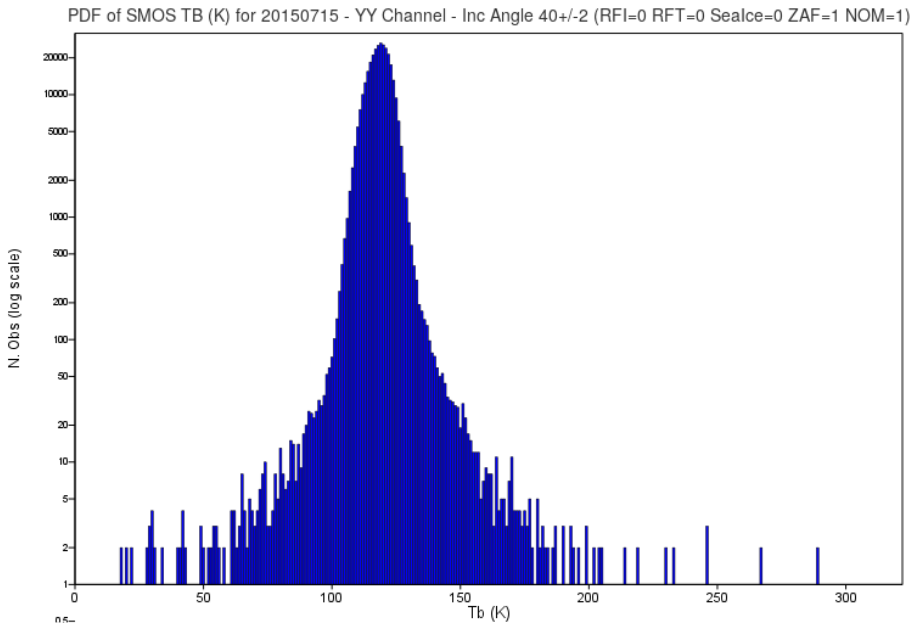

Figure 3: Similar to Fig. 1, but only where RFI and RFT flags are zero, ZAF is one and NOM is one 1, and there is no sea-ice contamination. The QC indicators are defined in Table 1.

The maps of the SMOS brightness temperature data presented in the histograms in Figure 1, Figure 2 and Figure 3 are respectively showed in Figure 4, Figure 5 and Figure 6. Based on the results in Figure 3 and for plotting purposes only data between 70 and 150 K is presented. Most of the observations (Figure 4) have brightness temperature values around 120-130 K which are located in the central part of the swath. Lower values, around 70 K, are found at the edge of the swath. Larger values, around 150 K, are found in some areas known to be contaminated by RFI (i.e. around China and South of Madagascar). Observations at the edge of the sea-ice areas show higher brightness temperature values due to sea-ice contamination.

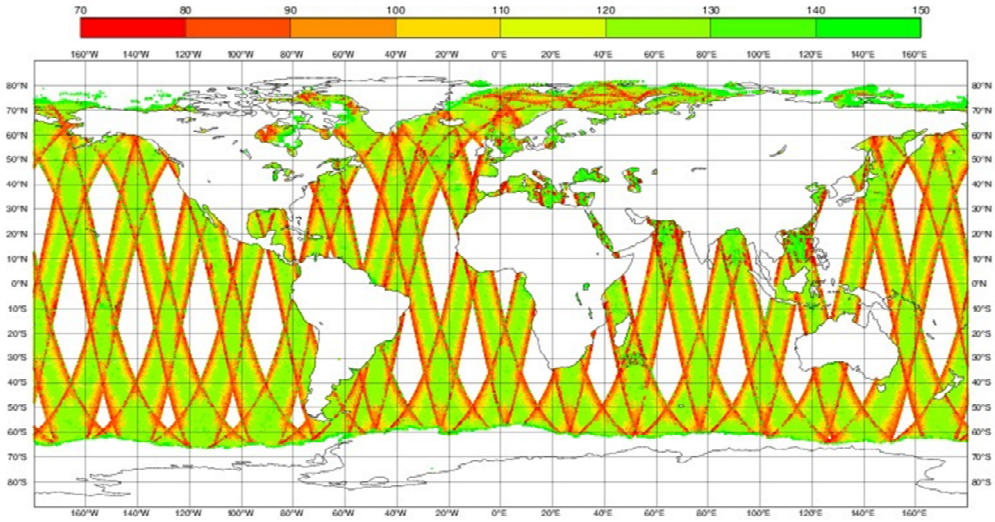

Figure 4: SMOS brightness temperature [K] map on 20150715 for the YY channel and incidence angles 40°±2°.

In Figure 5 shows the observations after the data contaminated by RFI is removed. There are now less observations with high value of brightness temperature. After the Alias Free area flag, the Overall quality flag (NOM) and the sea-ice contamination checks are applied (Figure 6) many of the outliers with very low values on the edge of the swath and the ones with high values at high latitudes are removed. Observations at the edge of the swath still show slightly lower values than the ones at the centre of the swath.

Only observations that passed all the flags and sea-ice check described above (the QC dataset) are compared to the CMEM and FASTEM simulated brightness temperatures.

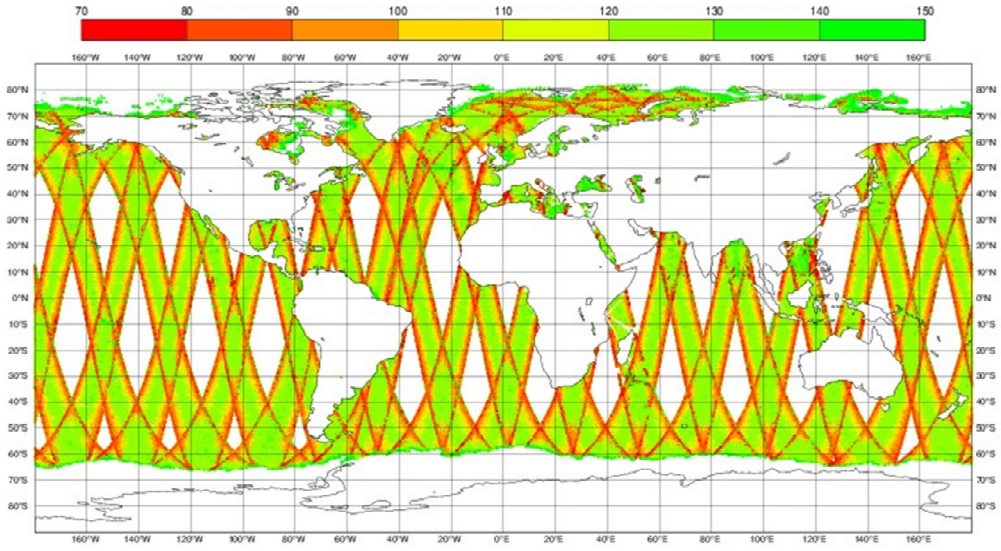

Figure 5: Similar to Fig. 4, but only where RFI and RFT flags are zero. The QC indicators are defined in Table 1.

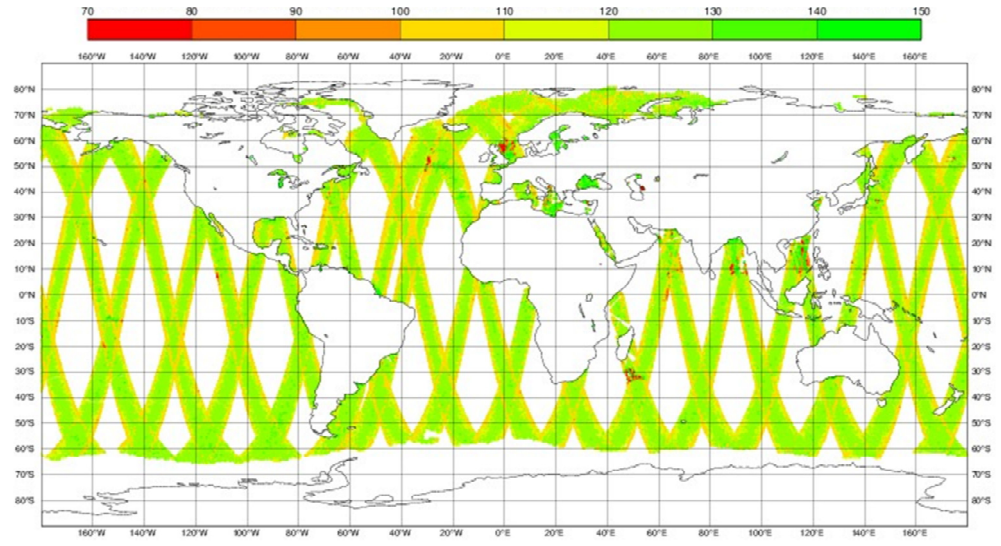

Figure 6: Similar to Fig. 4, but only where RFI and RFT flags are zero, ZAF is one and NOM is one 1, and there is no sea-ice contamination. The QC indicators are defined in Table 1.

5. SMOS simulated Tb with RTTOV-FASTEM

An off-line tool developed at ECMWF is available for computing the observation-minus-background departures or observation-minus-analysis departures of brightness temperatures using RTTOV-FASTEM based model equivalents.

The tool was adapted to be able to process SMOS brightness temperature observations. The code to transform simulated brightness temperatures from the Earth's to the antenna's reference frame is available in the SMOS processing code of IFS. This code was integrated into the RTTOV-FASTEM and used to rotate the SMOS model equivalent brightness temperature from the Earth reference frame to the satellite reference frame.

Several versions of RTTOV and FASTEM were tested. It was decided to align the off-line tool to the RTTOV-FASTEM version used in operation, i.e. RTTOV v12.1 with FASTEM v6. The differences among the various versions of RTTOV are described in Saunders et al., 2018.

5.1. FASTEM versus CMEM

CMEM simulated L-band brightness temperatures are available as output of the SMOS monitoring at ECMWF for each SMOS observation. As described in Section 3, in CMEM the ocean surface is considered as flat therefore the ocean roughness is not accounted for. FASTEM has the wind speed as input to model the emissivity due to the ocean roughness and foam. So, the two models are expected to give different results in windy conditions.

At ECMWF both FASTEM and CMEM are currently set up with a fixed global value of sea surface salinity (SSS). The global average value of SSS is set to 35 psu. In CMEM the SSS is set to 32.5 psu. CMEM was developed for land applications, and the sea surface was only contributing to Tb when a fraction of open water was present. The coastal areas and inland waters would justify an SSS value lower than the global average. FASTEM was first tested using the same SSS as CMEM. Then the average value of 35 psu was tested. Results are presented in the next Section.

5.2. Setting up FASTEM

To make a fair first comparison of the two models, FASTEM was run for 1 day (1st June 2015) with zero wind input. To align the two models, FASTEM was also run with an SSS value of 32.5 psu (FASTEM_WS0_SSS325). Due to the large size of the files, the comparison was limited to the latitude range [45°N – 45°S] to speed up the testing phase. In Figure 7 the map of the simulated brightness temperature differences between CMEM and FASTEM_WS0_SSS325 is shown for YY channel and incidence angles between 30 and 40 degrees. For zero wind conditions the differences between the two models are in the range of 1.5 - 2.5 K.

To evaluate the model differences due to the wind effect, FASTEM was run again for the 1st June 2015 with SSS=32.5 psu and ECMWF model background wind input used (FASTEM_SSS325). In Figure 8 the background winds at SMOS observation location for the 1st June 2015 as used by FASTEM are shown. Results of the comparison between FASTEM_SSS325 and CMEM are presented in Figure 9. When the wind is accounted for in FASTEM, the differences between the two models are, as expected, larger. There is clearly strong correlation between wind speed and CMEM/FASTEM_SSS325 differences. The differences range between 1.5 and 4.5 K, with larger values in areas with strong winds.

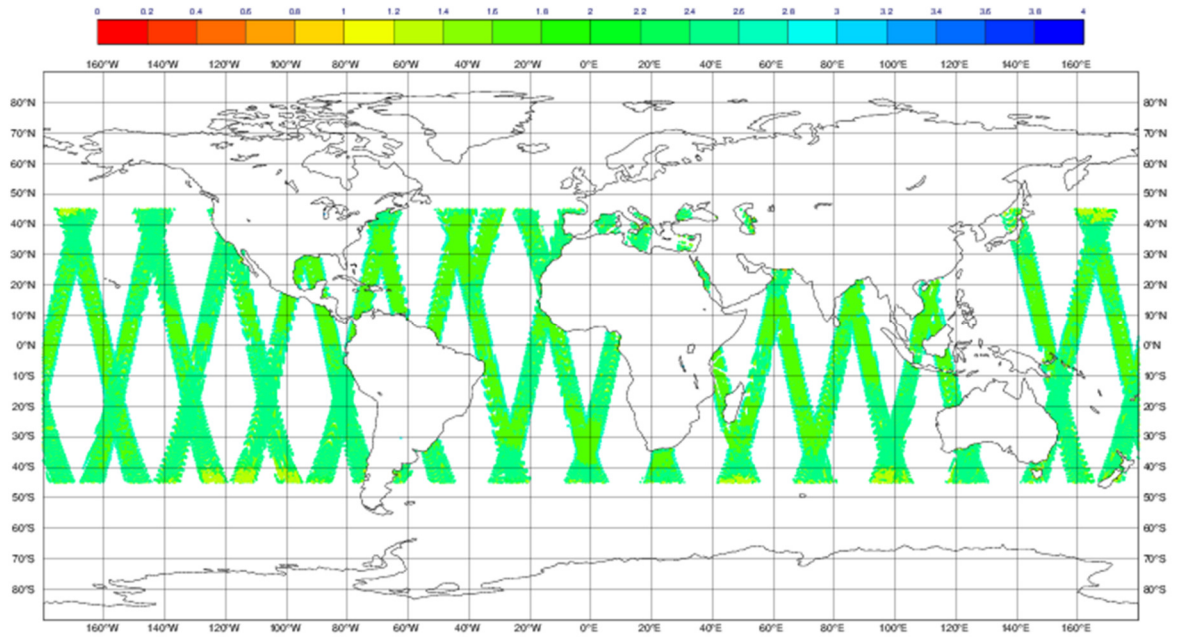

Figure 7: FASTEM_WS0_SSS325-CMEM simulated brightness temperature differences over the area 45°N - 45°S for the YY channel and incidence angle in the range 30-40 degrees when FASTEM and CMEM has both an SSS of 32.5 psu. FASTEM has zero wind input. CMEM values are not available for a descending orbit over Japan and Australia.

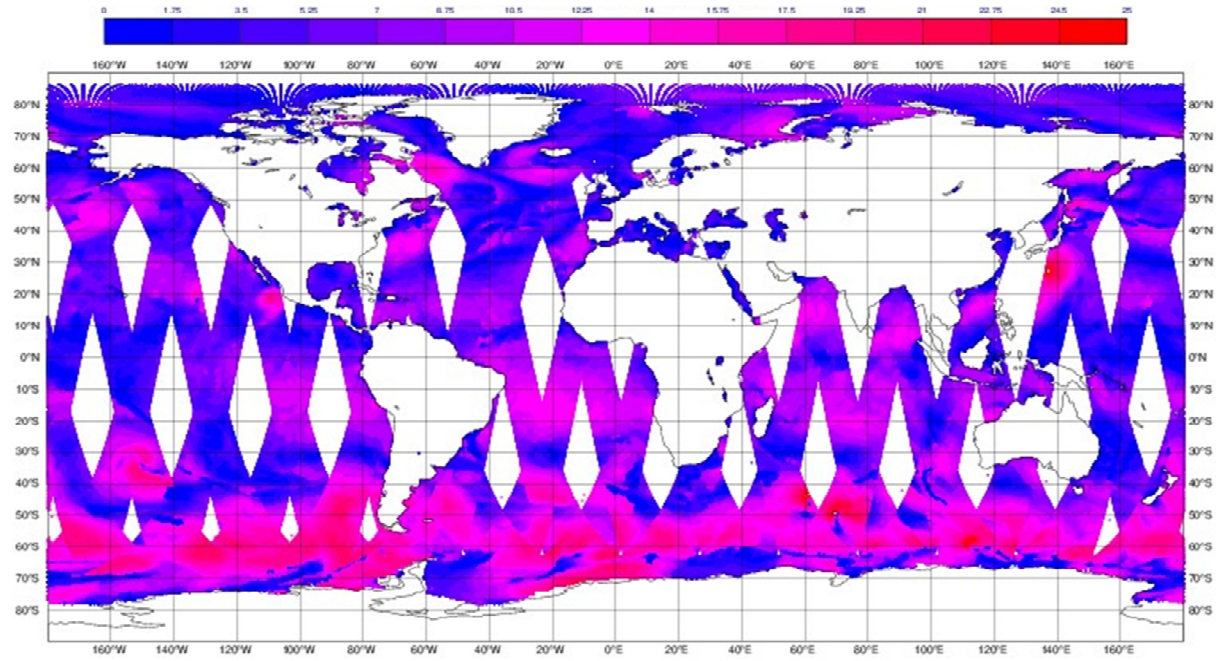

Figure 8: Background wind speed at SMOS observation locations for the 1st June 2015.

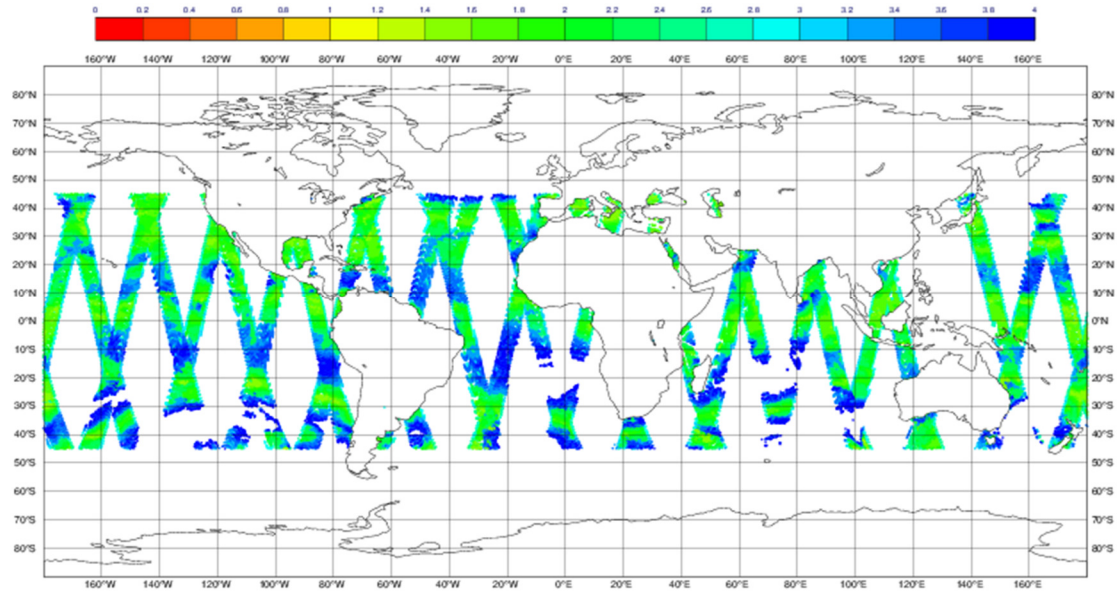

Figure 9: FASTEM_SSS325-CMEM simulated brightness temperature differences over the area 45°N - 45°S for the YY channel and incidence angle in the range 30-40 degrees. FASTEM and CMEM SSS is 32.5 psu. Background winds (from Fig. 8) were used as input to FASTEM.

In the next experiment FASTEM was run using the SSS set to the average global value of 35 psu (FASTEM_SSS35). FASTEM_SSS35 is closer to CMEM (see Figure 10) than FASTEM_SSS325. The differences are between 0 and 4.5 K with the highest values in areas with stronger winds. FASTEM simulated Tb is always stronger than the CMEM one.

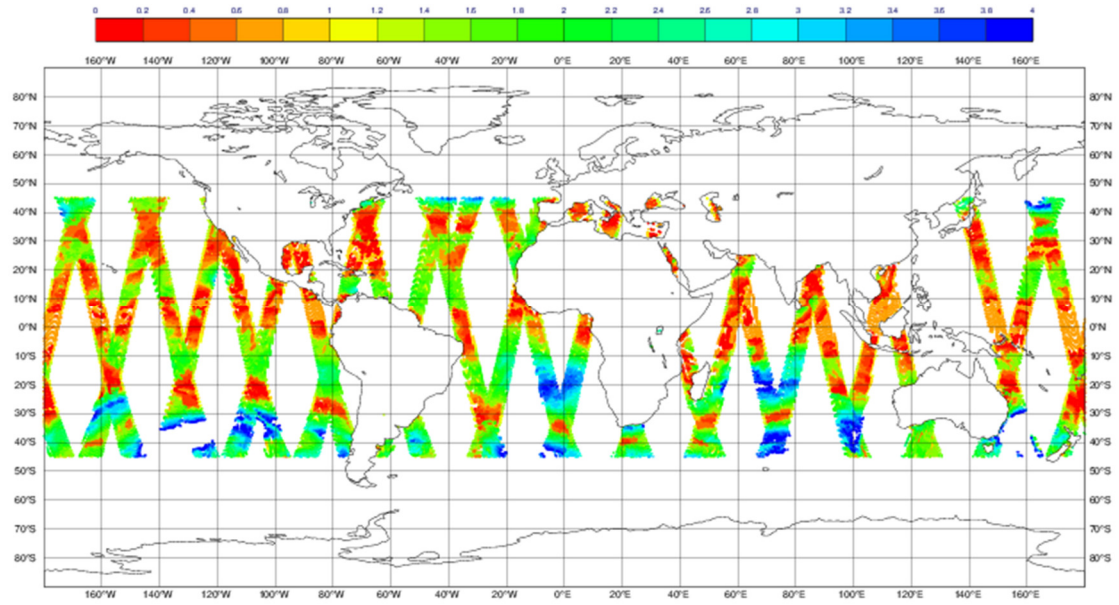

Figure 10: FASTEM_SSS35-CMEM simulated brightness temperature differences over the area 45°N - 45°S for the YY channel and incidence angle in the range 30-40 degrees. First-guess winds were used into FASTEM.

In zero wind speed conditions we found systematic differences between the two models using the same SSS value. We found by chance that FASTEM with SSS set to 35 psu is closer to CMEM used in operation (with SSS set to 32.5 psu). Several investigations were performed to understand this result, but a clear reason was not found.

CMEM and FASTEM do not use the same dielectric model. An offline calculations found the differences arising from this are small (maximum differences 0.5 K). However, FASTEM does not assume zero roughness at zero windspeed. On average there will be large scale roughness even with zero wind (from the mean ocean swell). This will also lead to non-zero FASTEM-CMEM differences at zero windspeed, as CMEM assumes a flat surface. It has also to be considered that FASTEM is a regression fit to the output of a model, so there will also be regression fit error arising from this which will be non-zero at zero windspeed. We could speculate that it happens that all these errors are going in the same direction, producing an apparent bias.

Since the global average SSS value is 35 psu, this value was used for the final configuration of FASTEM in this study.

5.3. FASTEM simulated brightness temperature

Once successfully tested, the tool was run over two months of SMOS data for the period June and July 2015. Two months of simulated L-band brightness temperature on top of the atmosphere were generated (at the SMOS observation location) using FASTEM starting from the ECMWF 6-hour forecast fields. For each observation, the departure from FASTEM brightness temperature was computed.

The simulated FASTEM (in the final configuration with SSS set to 35 psu) brightness temperatures were more extensively compared to the CMEM (with SSS set to 32.5 psu) brightness temperatures, taking into account different incidence angles and polarizations. The FASTEM-CMEM differences are plotted, globally for one day of data, 15th July 2015, for the YY-pol (Figure 11) and XX-pol (Figure 12) and incidence angles of 30°±2° (top panel) and 50°±2° (bottom panel), respectively. The differences between the two models are quite similar for both polarizations at low incidence angles (around 30°), being globally on average about 1K. At higher incidence angles (around 50°) the differences are larger due to the higher sensitivity of FASTEM to the wind speed. The difference is on average around 1.7 K in YY-pol and 3.1 K in XX-pol. On the 15th July a tropical cyclone (TC) was present off the coast of Baja California. As expected, the FASTEM simulated brightness temperatures over the TC are much larger than the CMEM ones.

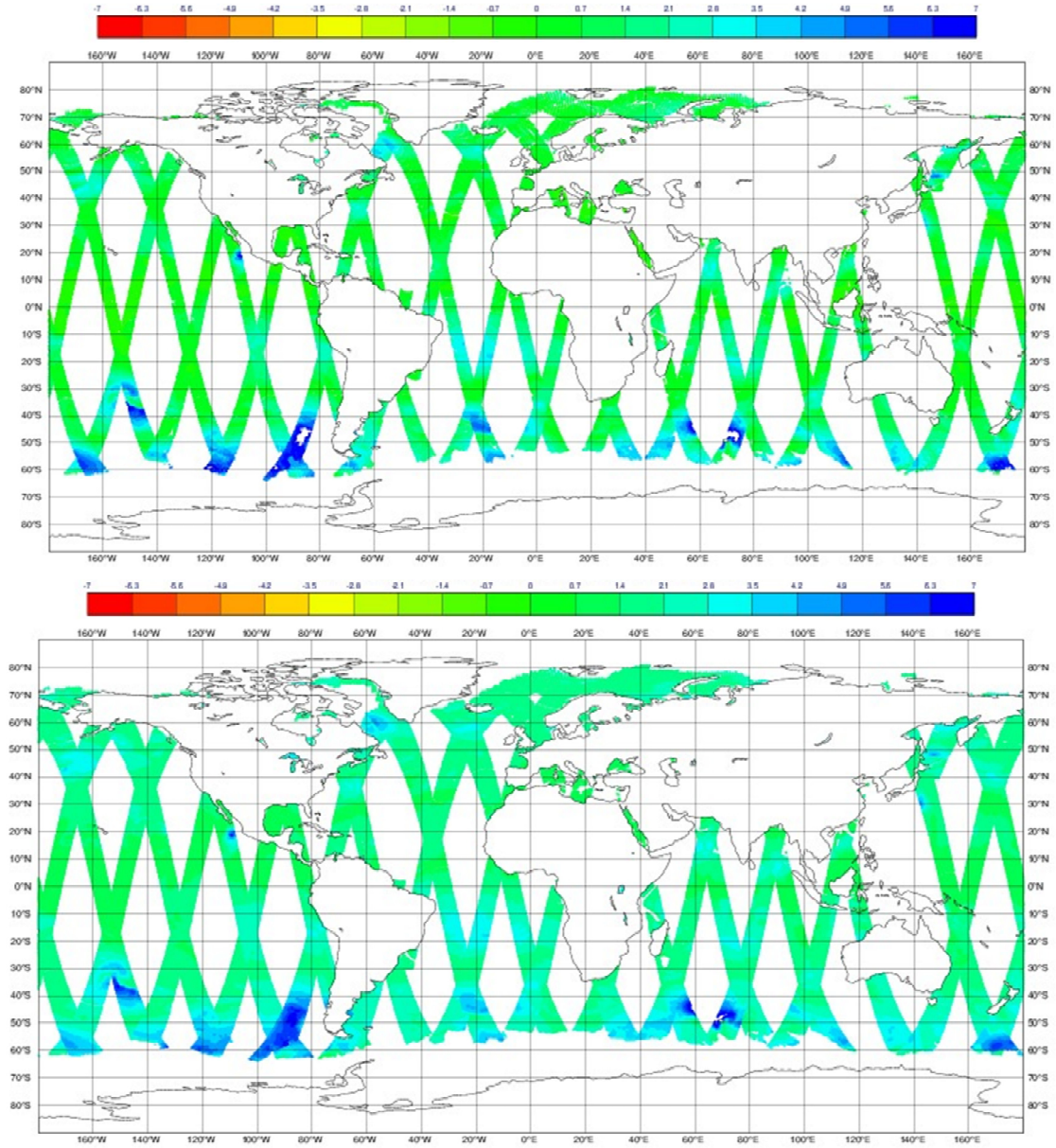

Figure 11: FASTEM-CMEM simulated brightness temperature differences on 15th July 2015: YY polarization; 30°±2° incidence angle (top panel) and 50°±2° incidence angle (bottom panel).

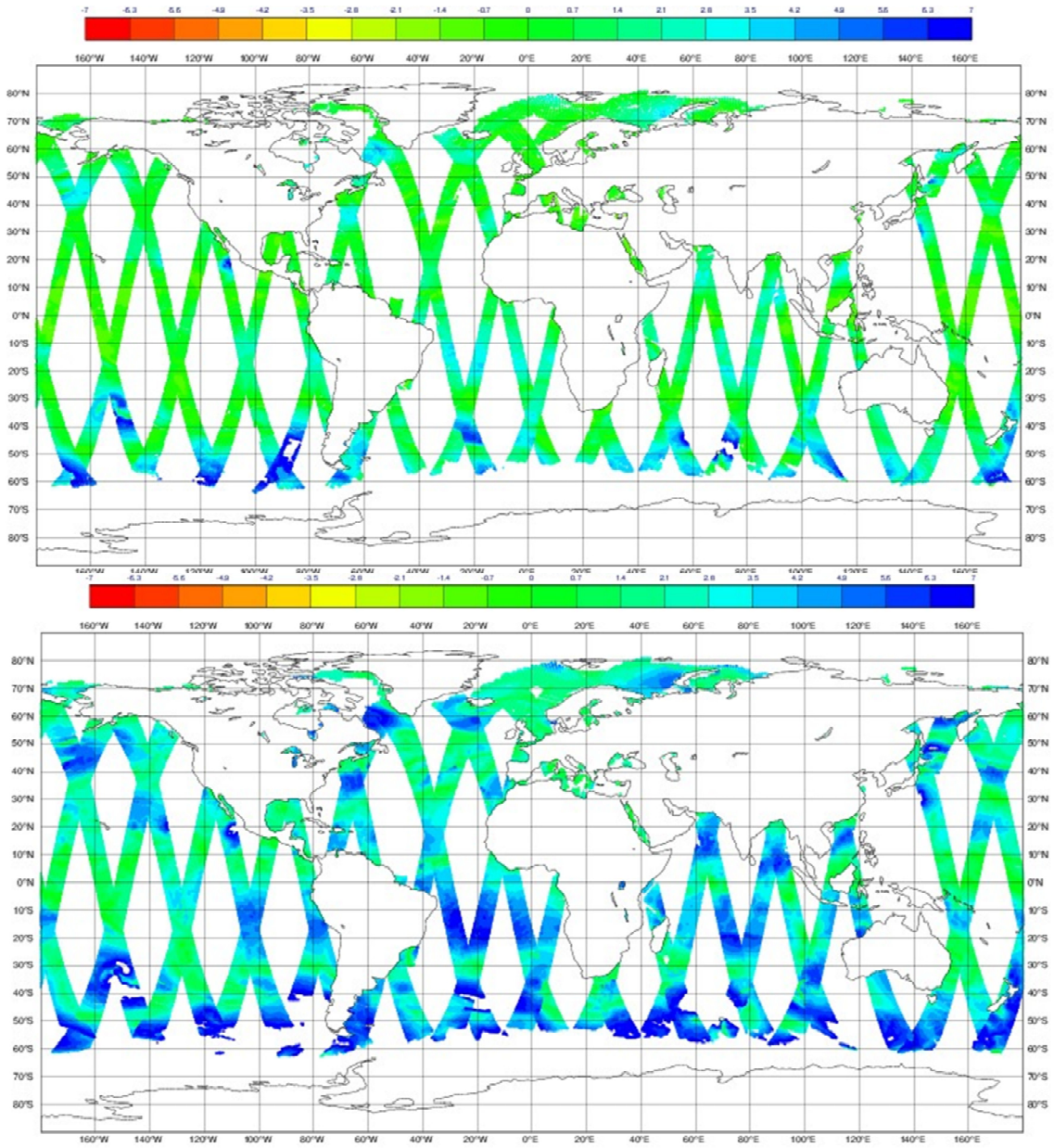

Figure 12: FASTEM-CMEM simulated brightness temperature differences on 15th July 2015: XX polarization; 30°±2° incidence angle (top panel) and 50°±2° incidence angle (bottom panel).

6. SMOS-FASTEM departures

The departures between SMOS and FASTEM were evaluated for the two polarizations at different incidence angles. Figure 13 and Figure 14 show the SMOS observed Tb for XX-pol and YY-pol, respectively, at two incidence angles: 30°±2° (top panels) and 50°±2° (bottom panels) for the 15th July 2015. The observations have passed the QC (as explained in Section 4). A difference in the Tb values between the observations at the centre of the swath and the ones at the edge of the swath is clear. This could be due to systematic residual errors that, in the SMOS ocean community, are treated applying the so-called Ocean Target Transformation (OTT), which is a type of bias correction [Gourrion et al., 2012]. Still few outliers are visible in the Mediterranean Sea, South of Madagascar, in the Chinese sea, due to RFI contaminated observations not completely removed by the QC.

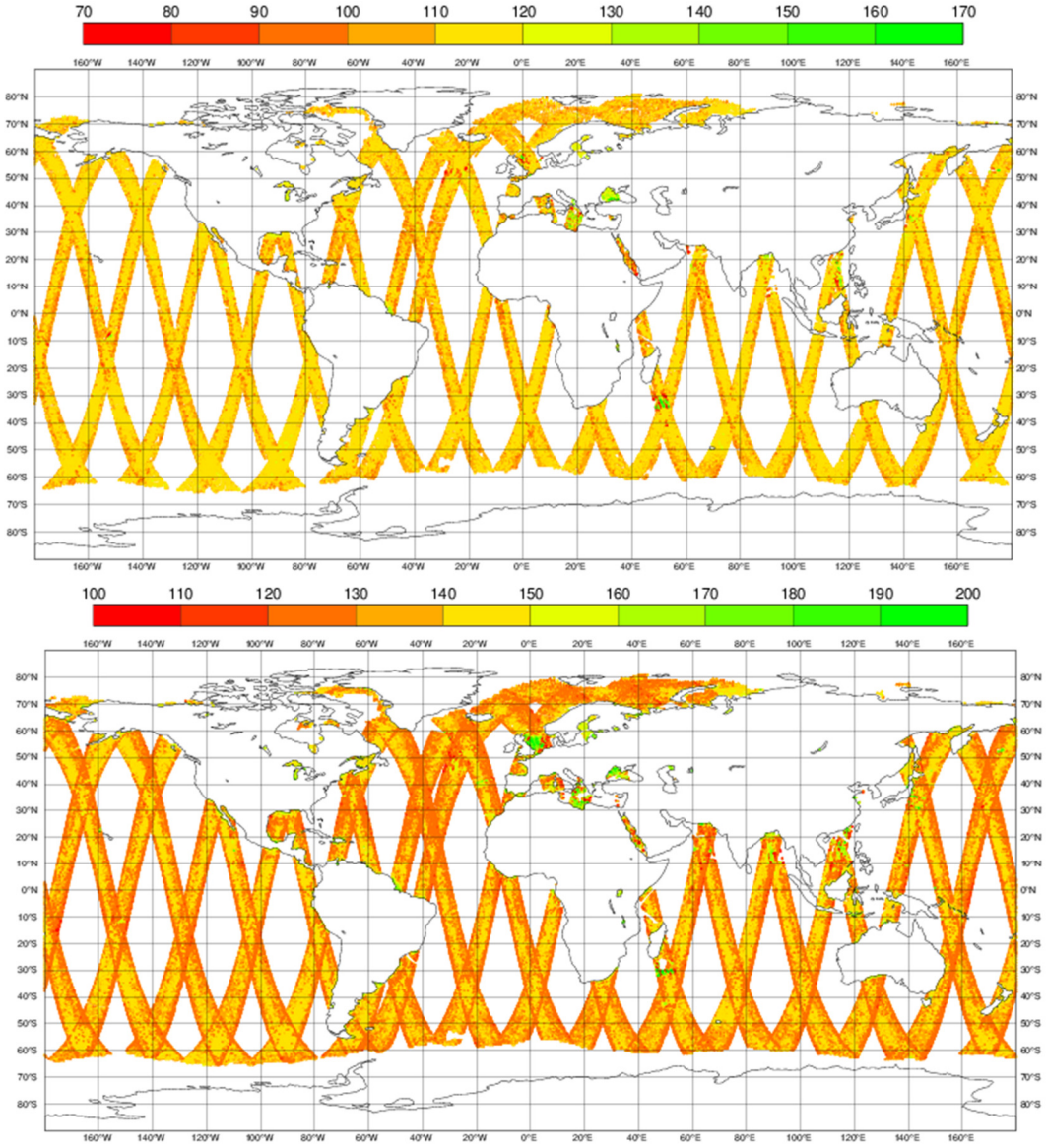

Figure 13: SMOS Tb [K] on 15th July 2015: YY polarization; 30°±2° incidence angle (top panel) and 50°±2° incidence angle (bottom panel).

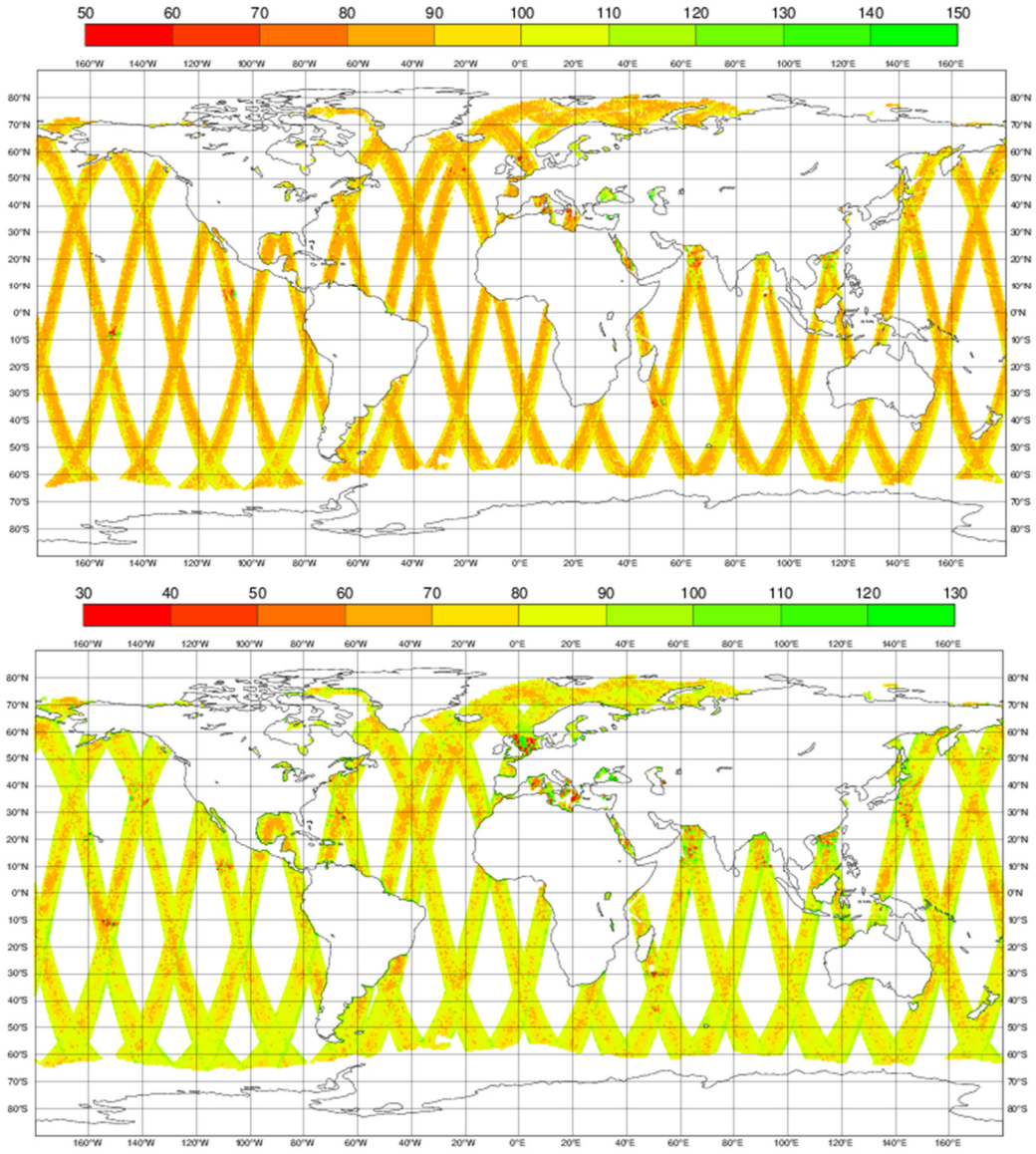

Figure 14: SMOS Tb [K] on 15th July 2015: XX polarization; 30°±2° incidence angle (top panel) and 50°±2° incidence angle (bottom panel).

Figure 15 and Figure 16 show the SMOS departures (SMOS-FASTEM) for YY-pol and XX-pol, respectively, at two ranges of incidence angles: 30°±2° (top panels) and 50°±2° (bottom panels) for the 15th July 2015. The SMOS departures for both polarizations are relatively small at low incidence angle in the centre of the swath, with values in the range of 0 to 2 K. XX-pol departures are smaller than YY-departures. The departures in the centre of the swath are larger at higher incidence angles, mainly at YY-pol. At the edge of the swath the departures are very large mainly at higher incidence angles. There are large departures in areas typically affected by RFI (e.g. around Europe and China). A bias correction applied to compensate for residual observation errors might reduce the departure between SMOS and FASTEM primarily at the edge of the swath.

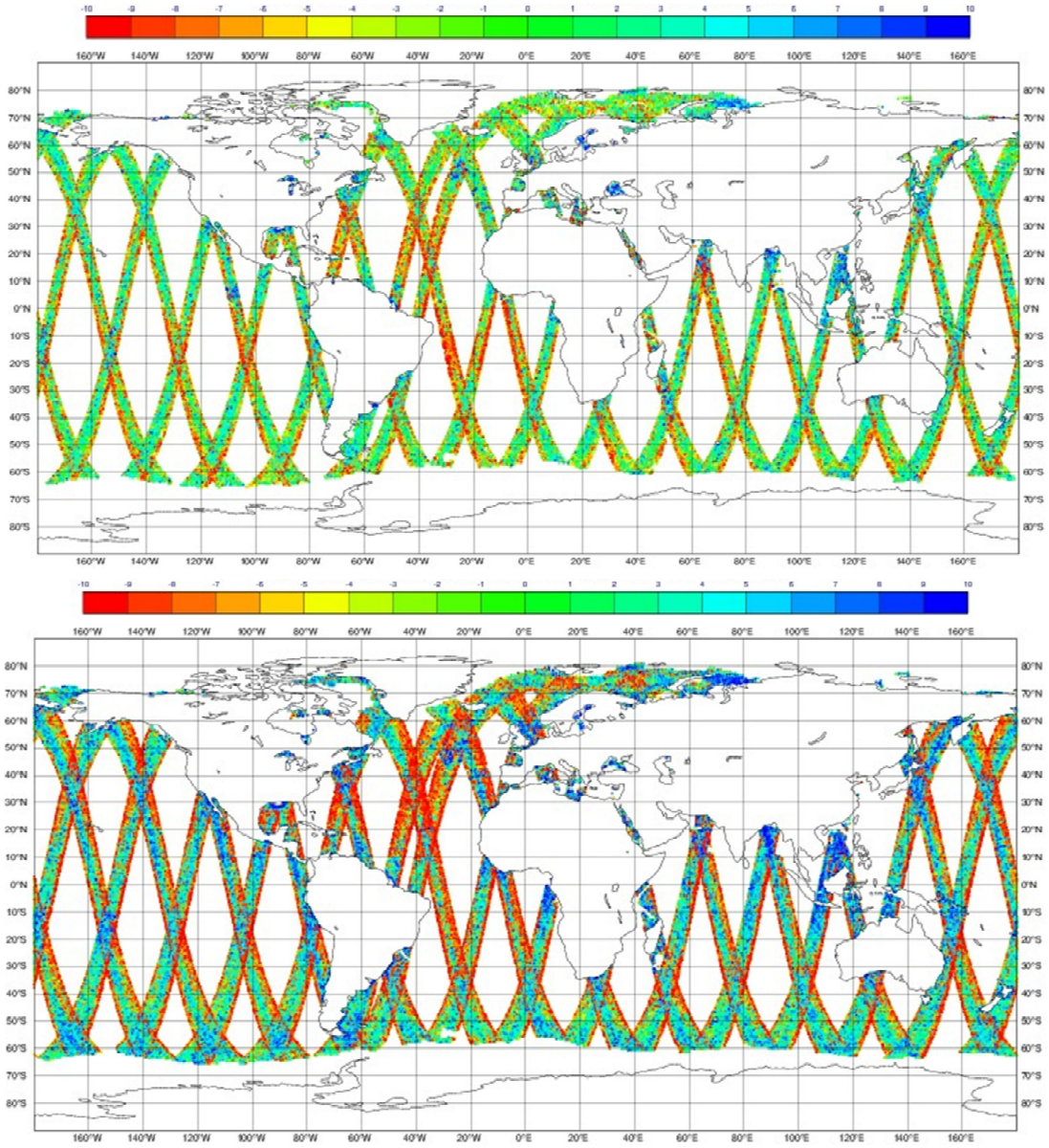

Figure 15: SMOS-FASTEM Tb differences [K] on 15th July 2015: YY polarization; 30°±2° incidence angle (top panel) and 50°±2° incidence angle (bottom panel).

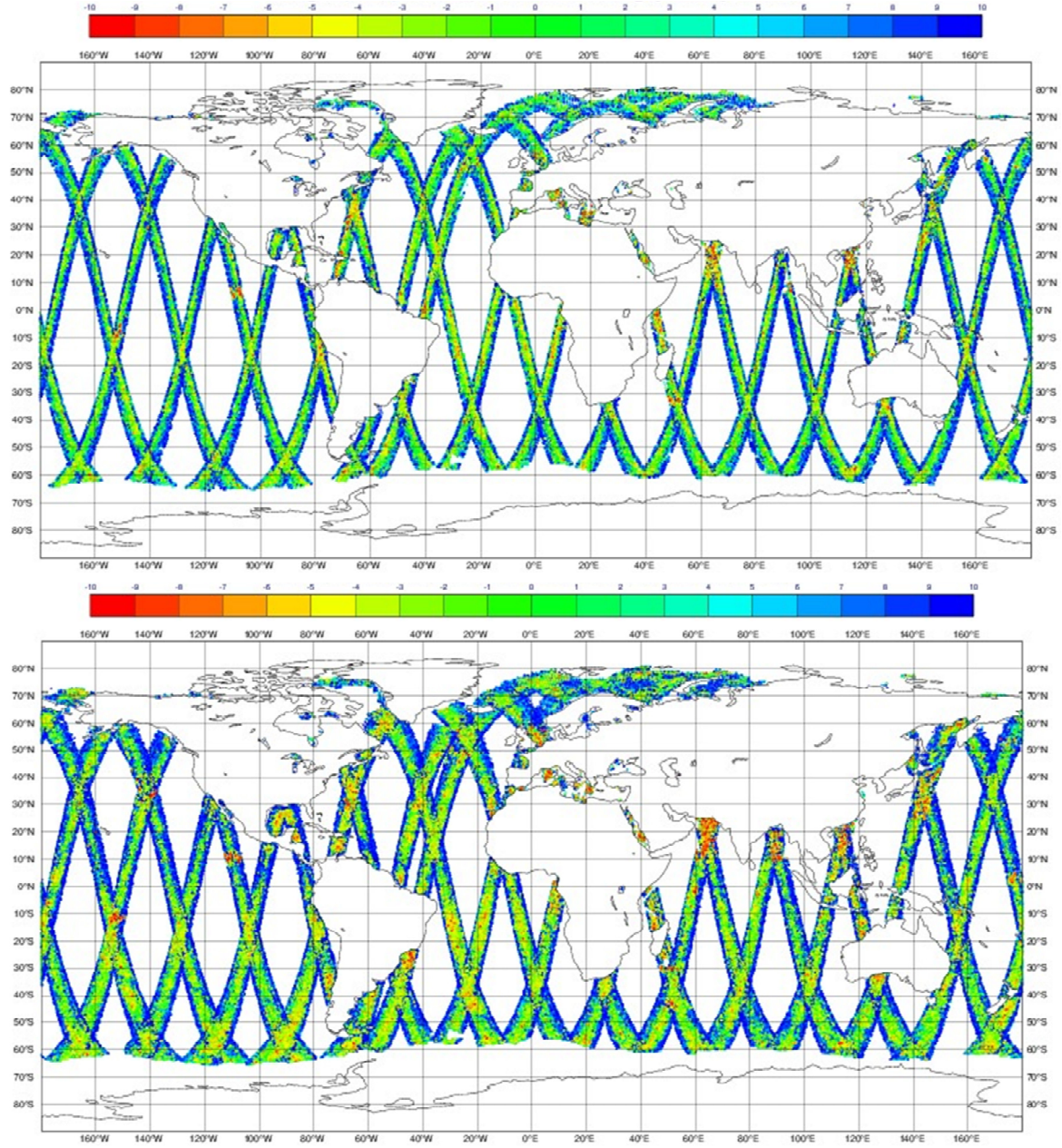

Figure 16: SMOS-FASTEM Tb differences [K] on 15th July 2015: XX polarization; 30°±2° incidence angle (top panel) and 50°±2° incidence angle (bottom panel).

The analysis of SMOS departures was extended to the full 2-month dataset (June-July 2015). Figure 17 and Figure 18 present the mean departures over 2 months for the YY-pol and XX-pol, respectively, at three different incidence angles: 30°±2° incidence angle (top panel), 40°±2° (mid panel) and 50°±2° incidence angle (bottom panel). Over 2 months the average SMOS Tb is smaller (by 3 to 4.5 K) than FASTEM at YY-pol, and stronger (by 3 to 6 K) than FASTEM at XX-pol. Very large biases are clear in the typical areas with RFI contamination like Europe and China. The standard deviation of the departures is around 8 K in YY-pol and 8.6 K in XX-pol. We believe that these values are strongly influenced by the observations characterized by large departure at the edge of the swath or affected by RFI contamination.

The standard deviation of the SMOS-CMEM departures (for the same period) is about 11 K in YY-pol and 11.5 K in XX-pol.

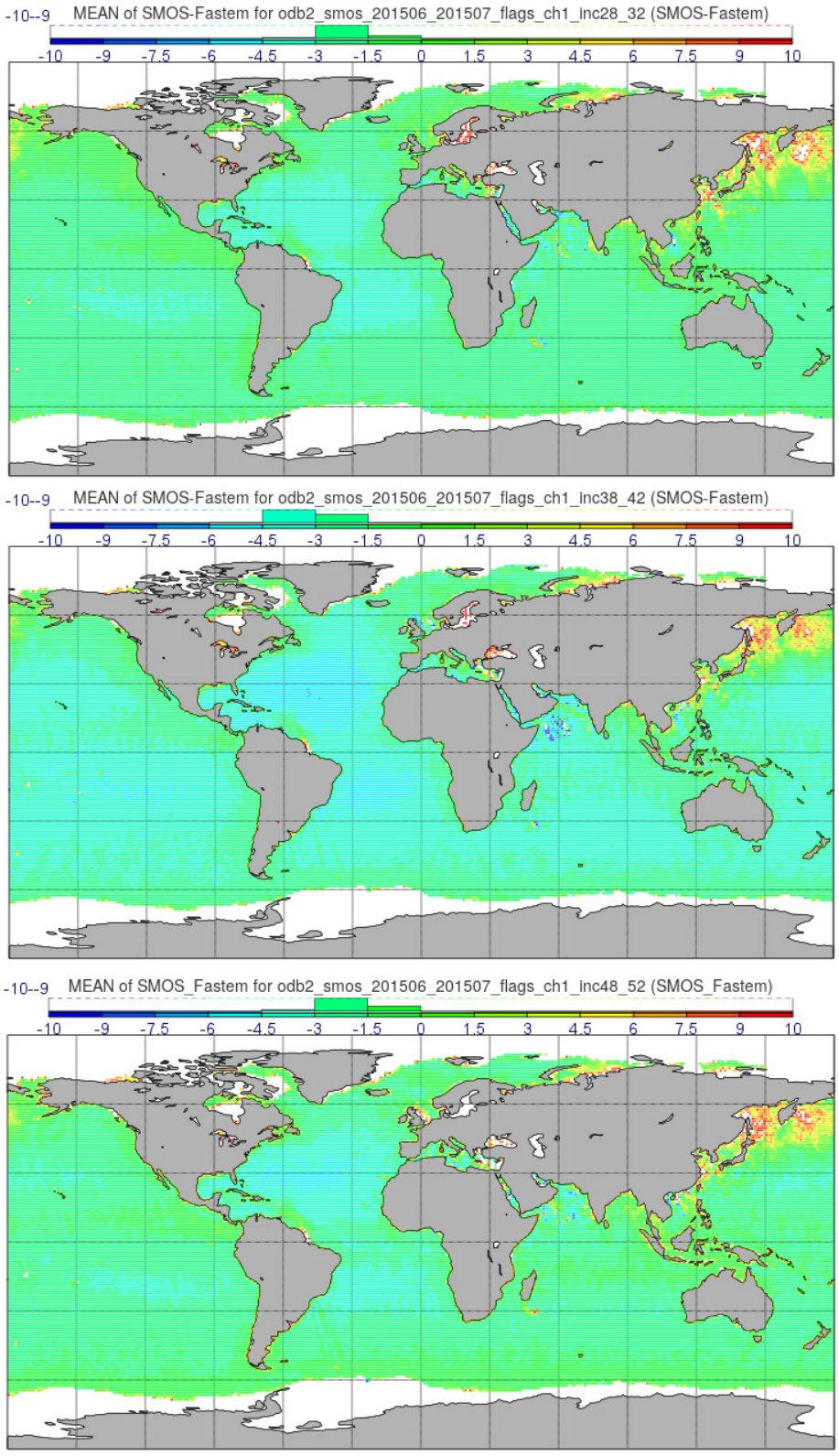

Figure 17: SMOS-FASTEM Tb differences [K] for June-July 2015: YY polarization; 30°±2° incidence angle (top panel), 40°±2° (mid panel) and 50°±2° incidence angle (bottom panel). The legend shows the histogram of the difference distribution.

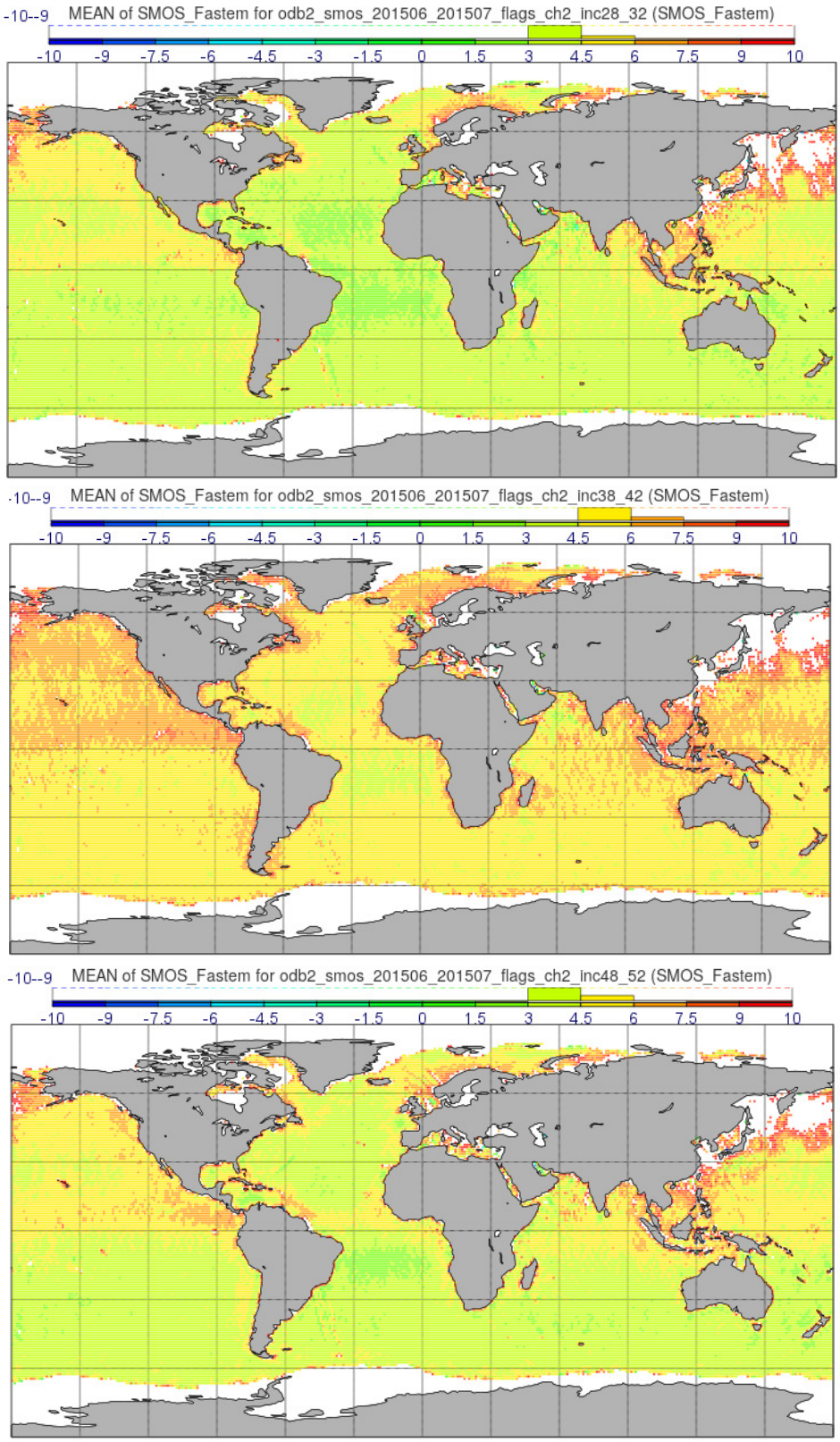

Figure 18: SMOS-FASTEM Tb differences [K] for June-July 2015: XX polarization; 30°±2° incidence angle (top panel), 40°±2° (mid panel) and 50°±2° incidence angle (bottom panel). The legend shows the histogram of the difference distribution.

7. FASTEM vs CMEM variability

The variability of the FASTEM and CMEM Tb was analysed and compared to SMOS Tb variability. This analysis was performed with the 2-month data extracted from an area less affected by RFI contamination. We selected an area in the South Pacific Ocean: 180W/90W/15S/60S.

A scatterplot of the FASTEM simulated Tb versus the SMOS observed ones is presented in Figure 19. SMOS shows a large variability (with the Tb ranging from 100 K to 120 K) which is partly due to the sea surface salinity and partially to the wind speed. FASTEM Tb have a slightly smaller variability: it seems quite good in capturing the wind variability (a subset of observations has increased Tb at increased SMOS Tb - small light blue data cloud). However, it cannot represent the variability due to the SSS as a constant salinity value was used (the large greenish cloud of data).

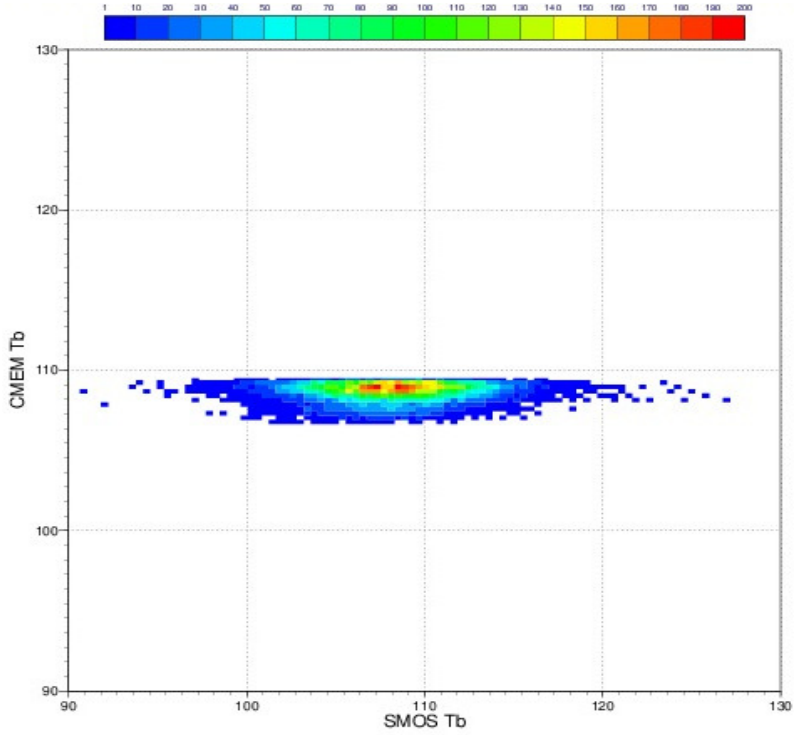

Figure 20 shows CMEM Tb versus SMOS one. CMEM has a very small variability and it does not capture the wind variability: there is a clear saturation of the signal.

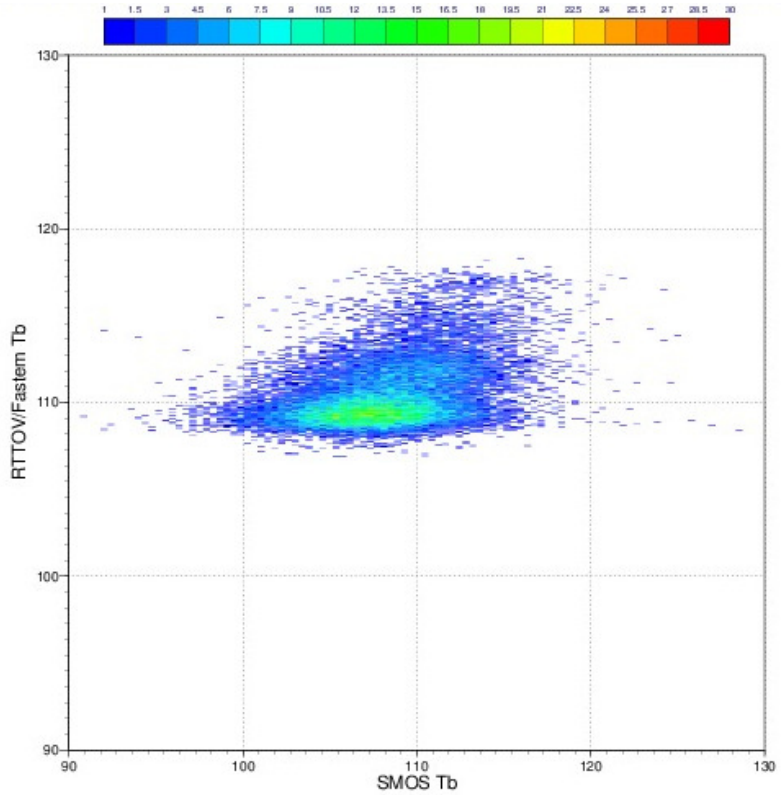

Figure 19: Scatterplot of FASTEM Tb versus SMOS Tb: YY polarization; 40°±2° incidence angle.

In this area the standard deviation of the SMOS-FASTEM departures are around 4.3 K in the YY-pol and 4.7 K at XX-pol. The SMOS-CMEM standard deviation of the differences are instead around 8 K at YY-pol and 9 K at XX-pol. This confirms that the global statistics are affected quite a lot by the RFI contamination.

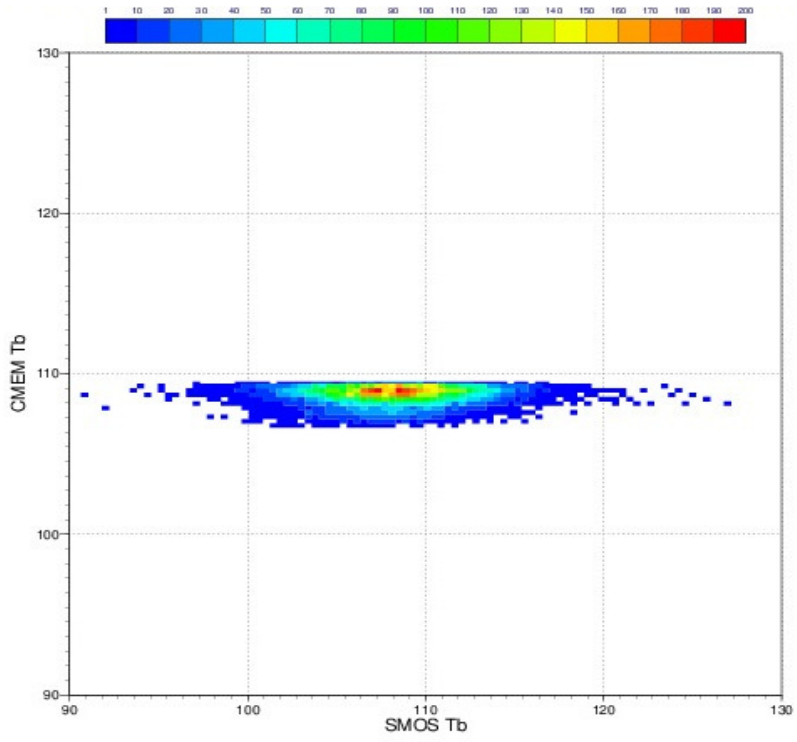

Figure 20: Scatterplot of CMEM Tb versus SMOS Tb: YY polarization; 40°±2° incidence angle.

8. Conclusions

In this study, preliminary investigations to improve the monitoring of SMOS brightness temperature over the ocean were completed. The simulated brightness temperature on top of the atmosphere at L-band was generated using FASTEM (as part of RTTOV) and transferred to the SMOS antenna reference frame. FASTEM is able to model the effects of the ocean roughness and foam. The FASTEM brightness temperatures were extensively compared to the CMEM ones to understand the differences between the two models. CMEM, which is currently used at ECMWF for passive monitoring over land and ocean, has a simple ocean emissivity model where the ocean is considered as a smooth surface. The simulated brightness temperature from FASTEM and CMEM were compared to the SMOS observed ones taking into account several factors like different viewing angle, polarization, RFI contamination. The simulated FASTEM brightness temperatures are closer to SMOS observations than the CMEM ones. This is seen also in case of extreme wind conditions like near tropical cyclones.

When comparing SMOS brightness temperatures to the modelled ones, FASTEM shows to be quite good in capturing the wind variability. CMEM, as expected, is not able to represent the wind variability. The effect of the variability due to the sea surface salinity has not been investigated in this study.

The SMOS-FASTEM average bias is around 4 K. The departure standard deviation is about 8 K. SMOS observations are still strongly affected by RFI contamination mainly in areas like Europe, China, Madagascar, USA. Observations affected by RFI can show departures up to 10-15 K. Such high values clearly affect the overall statistics. The RFI contamination is still a big issue in the SMOS community. A lot of effort has been put over a number of years to find a way to mitigate it. An improvement is expected with the next SMOS operational processor version v740. SMOS–FASTEM departures are small in the centre of the swath but are quite large at the edge of the swath. This is partially due to sun glint and direct sun contamination which affect the SMOS measurements mainly at the external part of the swath [Reul et al., 2007]. The SMOS observations affected by these effects could be removed by applying a tighter QC based on the flags provided in the BUFR files. A geometrical effect is also causing brightness temperatures values much higher or smaller than at the centre of the swath. In the SMOS community an OTT (Ocean target transformation) [Yin et al., 2014] is applied to compensate for this effect. The OTT is a form of bias correction measured over an area in the South East Pacific Ocean. An alternative form of bias correction for NWP applications could be the Variational Bias Correction (VarBC) [Dee, 2004]. Another radiation source at L-band is the galactic noise [Le Vine and Abraham, 2004]. The L1 SMOS observations are corrected only for the direct component of the galactic noise. The reflected component can be only corrected based on the wind induced ocean surface roughness and this is not taken into account of in this study. This could explain part of the bias between the two models and the observations. This is actually another potential advantage of using RTTOV instead of CMEM: since it is able to take the wind effect into account it has the potential to include a module that corrects for the reflected component of the galactic noise.

The monitoring of SMOS brightness temperature over the ocean would definitely benefit from using a forward model operator such as RTTOV-FASTEM.

Acknowledgements

We would like to thank Matthias Drusch and Susanne Mecklenburg (ESA) for their contribution in the project definition, Raffaele Crapolicchio (Serco Spa - ESRIN) for the clarifications of the SMOS products, Cristina Lupu and Marco Matricardi for their help with RTTOV and the monitoring tool, Joaquin Muñoz Sabatier and Patricia de Rosnay for their support on CMEM and the SMOS ODB products.

References

De Chiara G., L. Isaksen, S. English, (2017). Evaluation of SMOS storms evolution wind speed demonstration database". *Report for ESA contract 4000101703/10/NL/FF/fk CCN6, Technical Report 1 (TR1).*

Dee, D.P., (2004). Variational bias correction of radiance data in the ECMWF system. *Proc. ECMWF Workshop on Assimilation of High Spectral Resolution Sounders in NWP*. ECMWF, Reading, UK, 97, 112.

de Rosnay, P., M. Dragosavac, M. Drusch, A. Gutiérrez, M. Rodríguez, López, N. Wright, J. Muñoz Sabater, R. Crapolicchio, (2012). "SMOS NRT BUFR specification"

de Rosnay, P., M. Drusch, J. Muñoz Sabater, (2009). SMOS Global surface emission model (2009), *ESA contract report MS1TNP1*, 2009.

Drusch, M., E. Wood, and T. Jackson, (2001). Vegetative and atmospheric corrections for soil moisture retrieval from passive microwave remote sensing data: Results from the Southern Great Plains, *Hydrology Experiment 1997. J. Hydromet*., 2, 181–192.

English, S. T. Hewison, (1998). A fast generic millimeter-wave emissivity model. *Proc. SPIE,* vol. 3503, pp. 288–300, 1998.

Font J., A. Camps, A. Borges, M. Martın-Neira, J. Boutin, N. Reul, Y. H. Kerr, A. Hahne, S. Mecklenburg (2010). SMOS: The Challenging Sea Surface Salinity Measurement From Space. *Proceedings of the IEEE, Volume: 98, , May 2010.*

Gourrion, J., R. Sabia, M. Portabella, J. Tenerelli, S. Guimbard, A. Camps (2012). Characterization of the SMOS Instrumental Error Pattern Correction Over the Ocean. *IEEE Geoscience and Remote Sensing Letters* Vol. 9, No. 4, July 2012

Kerr YH, P. Waldteufel, J.P. Wigneron, J. Martinuzzi, J. Font, M. Berger (2001). Soil moisture retrieval from space: The Soil Moisture and Ocean Salinity (SMOS) mission. *IEEE Trans. Geosci. Remote Sens.* **39**: 1729-1735.

Kerr, Y., Waldteufel, P., Wigneron, J.P., Delwart, S., Cabot, F., Boutin, J., Escorihuela, M.-J., Font, J., Reul, N., Gruhier, C., Juglea, S., Drinkwater, M., Hahne, A., Martin-Neira, M., Mecklenburg, S. (2010). The SMOS mission: new tool for monitoring key elements of the global water cycle. *Proceedings of the IEEE, 98 (5), 666-687. DOI : 10.1109/JPROC.2010.2043032.*

Le Vine, D. M., S. Abraham, (2004). Galactic Noise and Passive Microwave Remote Sensing From Space at L-Band. *IEEE Transactions on Geoscience and Remote Sensing*, Vol. 42, No. 1, January 2004.

Liu, Q., F. Weng, S.J. English, (2011). An Improved Fast Microwave Water Emissivity Model. *IEEE Transaction on Geoscience and Remote Sensing*, Vol. 49, No. 4, April 2011.

McMullan KD, MA. Brown, M. Martin-Neira, W. Rits, S. Ekholm, J. Marti, J. Lemanczyk (2008). SMOS: The payload. *IEEE Trans. Geosci. Remote Sens.* **46**: 594-605.

Mecklenburg S., M. Drusch, Y. H. Kerr, J. Font, Manuel Martín-Neira, S. Delwart, G. Buenadicha, N. Reul, E. Daganzo-Eusebio, R. Oliva, R. Crapolicchio (2012). ESA's Soil Moisture and Ocean Salinity Mission: Mission Performance and Operations. *IEEE Transactions On Geoscience And Remote Sensing,* Vol. 50, No. 5, May 2012.

Muñoz-Sabater J., P.de Rosnay, M. Dahoui (2011a). SMOS continuous monitoring report - Part 1. *ESA Contract Report.*

Muñoz-Sabater, J., M. Dahoui, P. de Rosnay, L. Isaksen, (2011b). *Technical Note Phase II WP1100: SMOS Monitoring Report.* Number 2: Nov 2010-Nov 2011

Muñoz-Sabater J, Fouilloux A, de Rosnay P. (2012). Technical implementation of SMOS data in the ECMWF Integrated Forecasting System. *Geosc.Remote Sens. Letters* 9(2): 252–256, doi:10.1109/LGRS.2011.2164777

Muñoz-Sabater J., P. de Rosnay, A.Fouilloux, M. Dahoui, L. Isaksen, C. Albergel, I. Mallas, T. Wilhelmssom, (2013). Tech. Note, Phase I: "*Final Report".* January 2013

Oliva, R., E. Daganzo, Y. Kerr, S. Mecklenburg, S. Nieto, P. Richaume, C. Gruhier (2012). SMOS Radio Frequency Interference Scenario: Status and Actions Taken to Improve the RFI Environment in the 1400-1427 MHz Passive Band. *IEEE Trans Geosci. Remote Sens., Special issue dedicated to SMOS*, May 2012. Vol. 50, N0 5, pp. 1427-1439

Reul, N., J. Tenerelli, B. Chapron, P. Waldteufel (2007). Modeling Sun Glitter at L-Band for Sea Surface Salinity Remote Sensing With SMOS. *IEEE Transactions on Geoscience and Remote Sensing,* Vol. 45, Issue 7, July 2007.

Reul, N., J. Tenerelli, B. Chapron, D. Vandemark, Y. Quilfen, and Y. Kerr (2012). SMOS satellite L-band radiometer: A new capability for ocean surface remote sensing in hurricanes. *J. Geophys. Res., 117, C02006,* doi:10.1029/2011JC007474.

Reul, N., B. Chapron, E. Zabolotskikh, C. Donlon, Y. Quilfen, S. Guimbard, J.F. Piolle (2015). A revised L-band radio-brightness sensitivity to extreme winds under Tropical Cyclones: the five years SMOS-storm database. *Remote Sensing of Environment, 180, 274–291,* doi:10.1016/j.rse.2016.03.011 274-291.

Saunders, R., Hocking, J., Turner, E., Rayer, P., Rundle, D., Brunel, P., Vidot, J., Roquet, P., Matricardi, M., Geer, A., Bormann, N., and Lupu, C., (2018). An update on the RTTOV fast radiative transfer model (currently at version 12). *Geosci. Model Dev., 11,* 2717-2737, https://doi.org/10.5194/gmd-11-2717-2018, 2018.

Wigneron, J.-P., Y. Kerr, P. Waldteufel, K. Saleh, M.-J. Escorihuela, P. Richaume, P. Ferrazzoli, P. de Rosnay, R. Gurney, J.-C. Calvet, M. Guglielmetti, B. Hornbuckle, C. Mätzler, T. Pellarin, and M. Schwank, (2007). L-band Microwave Emission of the Biosphere (L-MEB) Model: description and calibration against experimental data sets over crop fields. *Remote sens. environ.*, 107, 639–655.

Yin, X., Boutin, J., Martin, N., Spurgeon, P., Vergely, J. -L., & Gaillard, F. (2014). Errors in SMOS sea surface salinity and their dependency on a priori wind speed. *Remote Sensing of Environment*,146,159–171.